Colloids and Surfaces B: Biointerfaces 75 (2010) 300–309

Contents lists available at ScienceDirect

Colloids and Surfaces B: Biointerfaces

journal homepage: www.elsevier.com/locate/colsurfb

A new approach for the *in vitro* identification of the cytotoxicity of superparamagnetic iron oxide nanoparticles

Morteza Mahmoudi[a,*], Abdolreza Simchi[a,b,*], Mohammad Imani[c], Mohammad A. Shokrgozar[d,*], Abbas S. Milani[e], Urs O. Häfeli[f], Pieter Stroeve[g]

[a] *Institute for Nanoscience and Nanotechnology, Sharif University of Technology, Tehran, Iran*
[b] *Department of Materials Science and Engineering, Sharif University of Technology, Tehran, Iran*
[c] *Novel Drug Delivery Systems Department, Iran Polymer and Petrochemical Institute, Tehran, Iran*
[d] *National Cell Bank, Pasteur Institute, Tehran, Iran*
[e] *School of Engineering, University of British Columbia Okanagan, Kelowna, Canada*
[f] *Faculty of Pharmaceutical Sciences, University of British Columbia, Vancouver, Canada*
[g] *Department of Chemical Engineering and Materials Science, University of California Davis, Davis, USA*

ARTICLE INFO

Article history:
Received 30 April 2009
Received in revised form 24 August 2009
Accepted 31 August 2009
Available online 4 September 2009

Keywords:
Iron oxide nanoparticles
SPION
Toxicity
DMEM
MTT

ABSTRACT

Superparamagnetic iron oxide nanoparticles (SPIONs) are increasingly used in medical applications, such as targeting delivery and imaging. In the future, patients are more likely to be exposed to pharmaceutical products containing such particles. The study of toxicity of SPIONs has become of great importance in recent years, although the published data in this arena is limited. The aim of the present work is to investigate the cytotoxicity of SPIONs and the effect of the particles on the cell medium components. For this purpose, uncoated and polyvinyl alcohol (PVA) coated SPIONs with narrow size distribution were synthesized via a well-known coprecipitation method. The mouse fibroblast cell line L929 was exposed to SPIONs to probe the toxicity of magnetic nanoparticles during the bio application. Changes to the cell medium caused by SPIONs were analyzed with zeta potential measurements, ultraviolet visible spectroscopy (UV/vis) and the 3-[4,5-dimethylthiazol-2yl]-2,5-diphenyltetrazolium bromide (MTT) assay. It is observed that gas vesicles are formed in SPION-treated cells. Toxicity is conventionally explained by changes in the DMEM's pH and composition due to the tendency of SPIONs to interact with biomolecules. A new procedure is proposed to examine the *in vitro* toxicity of nanoparticles in a more rigorous manner, which gives an improvement in the relationship between *in vivo* and *in vitro* toxicity studies.

1. Introduction

The efficiency of cancer chemotherapy depends not only on the anticancer agent used, but also on the manner that it is delivered to target tissues and cancer cells [1,2]. Nanotechnology has offered new alternatives for cancer diagnosis and targeted treatments because of the unique properties of nanoscale structures. Such nanoscale structures include gold, iron oxides (i.e., magnetite and maghemite) and titanium oxide. Recent reports demonstrate that drug-coated polymeric nanospheres and nanocapsules can increase intracellular anticancer effects [8–11]. Furthermore, new nanocomposites are used for DNA detection [3], intracellular labeling [4], drug delivery [5], cancer targeting [6] and imaging [7].

For *in vivo* applications, it is of utmost importance that nanoscale structures are biocompatible. In nanoparticles, for example, it is important that the coating is non-toxic and insulates the body from undesired toxic side effects. Specifically, researchers have studied undesired toxic side effects, often with a focus on metals and metal oxide nanoparticles [11–15]. Jeng and Swanson [11] have reported changes in cellular morphology, mitochondrial function, membrane leakage (by lactate dehydrogenase (LDH)), permeability of plasma membrane and apoptosis after exposing cells to several types of metal oxide nanoparticles. Zinc oxide particles were found to be the most potent. Hussain et al. [13] showed toxic effects on cellular morphology, mitochondrial function (3-[4,5-dimethylthiazol-2yl]-2,5-diphenyltetrazolium bromide (MTT) assay), membrane leakage of lactate dehydrogenase (LDH assay), reduced glutathione (GSH) levels, reactive oxygen species (ROS) and mitochondrial membrane potential (MMP) after exposure of rat liver cells to Ag nanoparticles. Fe_3O_4 and TiO_2 nanoparticles, however, were shown to be much

* Corresponding authors.
E-mail addresses: Mahmoudi@mehr.sharif.edu (M. Mahmoudi), simchi@sharif.edu (A. Simchi), mashokrgozar@pasteur.ac.ir (M.A. Shokrgozar).

0927-7765/$ – see front matter © 2009 Elsevier B.V. All rights reserved.
doi:10.1016/j.colsurfb.2009.08.044

less toxic [13]. Veranth and co-workers [15] studied the cytokine response in BEAS-2B cells due to metal oxide nanoparticles and found that metal oxide particles have a lower toxicity than an equal mass of micron-sized particles of the same nominal composition.

The successful drug delivery and transfections can have massive academic, clinical, and practical impacts on gene therapy, cell and molecular biology, pharmaceutical and food industries, and bioproduction [16–18]. Targeting specific sites *in vivo* for the delivery of therapeutic agents presents a major obstacle to the treatment of many diseases, including cancer. A targeted delivery technique that has gained prominence in recent years is the use of magnetic nanoparticles. In these systems, therapeutic agents are attached to biocompatible magnetic nanoparticles and magnetic fields generated outside the body are focused on specific targets *in vivo* [19,20]. Superparamagnetic iron oxide nanoparticles (SPIONs) are promising candidates in a number of biomedical applications, including enhanced resolution magnetic resonance imaging (MRI), hyperthermia, drug delivery, tissue repair, cell and tissue targeting and transfection [21,22]. The potential of SPION in these applications is due to their small size (below 30 nm), their superparamagnetic properties, and their generally good biocompatibility. Not all researchers, however, seem to agree on the non-toxicity of SPIONs, and different assays have been used to investigate these concerns. The MTT assay has been used to measure the toxicity of SPIONs [19–21]. One of the toxic effects induced by nanoparticles is their ability to cause oxidative stress [23,24]. There is a link between DNA damage, mutations and cancer, and nanoparticles that are potent in causing this damage are more likely to have an adverse effect in cancer development. Reported studies on the effect of nanoparticles on DNA damage and oxidative stress are scarce [25].

In general, it is preferable to investigate the toxicity of nanoparticles with *in vitro* assays because they are simpler, faster, more cost effective and pose no ethical problems compared to *in vivo* studies. However, researchers found little correlation between *in vivo* and *in vitro* toxicity results, especially with using nanoparticles [26]. Toxic responses were observed for nanoparticles *in vitro* [27] but the same results were not exactly reproduced *in vivo* [28]. One possible reason for this discrepancy may be that during *in vivo* assays, there will be few detectable changes observed due to the well-known principle of body homeostasis. However; there is no such phenomenon *in vitro*. This toxicological finding is not so far from its pharmacologic analogy where *in vitro* results may not support *in vivo* results. The poor correlation between the toxicity measurement methods for *in vivo* and *in vitro* may also be due to the ability of nanoparticles to change the cell medium during *in vitro* assays, for example by protein/ion adsorption and pH changes, caused in part by the SPIONs surface activity. In contrast, during *in vivo* assays, changes in the surrounding tissues do not occur to the same extent when identical amounts of nanoparticles are applied. As a more specific example, the kidneys are able to filter blood and produce urine, thereby regulating the water and ion concentrations of blood plasma. Besides excreting nitrogen compounds, toxins, water, and electrolytes, kidneys also act as endocrine organs by secreting the hormones erythropoietin, renin and prostaglandins [29]. In order to obtain comparable results between the *in vivo* and *in vitro* cytotoxicity of SPIONs, the effects of SPIONs on the cell culture medium should be probed.

The aim of this study is to advance the study of the cytotoxic effects of magnetite nanoparticles and to probe their ability to change cell culture medium compositions. To this end, the mouse connective tissue cells L929 were used and toxicity levels and changes in the cell culture medium compositions due to SPIONs exposure were determined using the MTT assay and UV/vis spectroscopy. A new procedure is proposed to examine the *in vitro* toxicity of nanoparticles that can lead to more reliable toxicity results.

2. Materials and methods

2.1. Particle preparation and characterization

Polyvinyl alcohol (PVA, M_W = 30,000–40,000, degree of hydrolysis 86–89%) and the dye crystal violet were purchased from Fluka (Switzerland). Analytical grade ferrous and ferric chloride ($FeCl_2$ and $FeCl_3$) and sodium hydroxide (NaOH) were purchased from Merck (Darmstadt, Germany) and used without further purification. Other chemicals were of analytical grade.

Solutions were prepared by bubbling argon through deionized (DI) water for 30 min for deaeration. Iron salts were dissolved in DI water containing 0.5 M HCl, with the mole fractions of Fe^{2+} to Fe^{3+} adjusted to 1:2 for all samples. Particle precipitation was performed by drop-wise addition of iron salt solutions to NaOH solutions under an argon atmosphere. To prevent the development of large polycrystalline particles, turbulence was created by placing the reaction flask in an ultrasonic bath (100 W) and controlling the homogenization (overhead stirrer) rate (3600–9000 rpm) during the initial two minutes of the reaction. Various reaction conditions, e.g., NaOH molarity and stirring rate, were varied to obtain a narrow size distribution [30]. To this end, the stirring rate of 9000 rpm and the base molarity of 1.2 were selected. After 30 min, a PVA solution (polymer to iron mass ratio of 2; this amount of polymer is able to create non-aggregated coated particles [31]) was added as a stabilizer, and the reaction was then allowed to proceed (3600 rpm, 35 °C) for an additional 30 min. The PVA coated SPION were subsequently collected by centrifugation at 2000 × *g* for 10 min and re-dispersed in DI water. The resulting ferrofluid was stored at 4 °C for future use.

The synthesized nanoparticles were characterized by various analytical techniques. Transmission electron microscopy (TEM) with a ZEISS model EM-10C operating at 100 kV was used for size and morphology characterization. X-ray diffraction (XRD) studies were carried out with a Siemens D5000 with Cu K_α radiation for phase characterization and particle size determination using the Scherrer method. Mean size of nanoparticles was determined by dynamic light scattering (DLS; Zetasizer model ZEN 1600, nano laser 633 nm). The magnetization of the samples in a variable magnetic field was measured using a vibrating sample magnetometer (VSM) with a sensitivity of 10^{-3} emu and a magnetic field up to 20 kOe. The magnetic field was changed uniformly with a time rate of 66 Oe/s. In addition, the surface charge of nanoparticles was measured with a ZetaPALS (Brookhaven).

2.2. Assessment methods for in vitro toxicity of nanoparticles

The L929 mouse fibroblasts from the Pasteur Institute, National Cell Bank of Iran (NCBI), were seeded on glass cover slips in 96 well plates with 10,000 cells inoculated per well in 150 μl of medium and incubated for 24 h. Cells were cultured in Dulbecco's modified Eagle's medium (DMEM) supplemented with 10% fetal bovine serum (FBS) at 37 °C in a 5% CO_2 incubator. After the 24 h incubation period, 20 μl of the media containing SPIONs and extract media of uncoated and coated SPIONs (400, 800 and 1600 mM iron (i.e., 14.5, 29 and 58 mg/ml, measured by atomic absorption) were added to the wells and the cells were further incubated for additional periods ranging from 24 to 48 and 72 h.

Since magnetic nanoparticles can accumulate at the targeted sites during a targeting application, it is worthwhile to evaluate their cytotoxicity at high concentrations. For this reason high concentrations of SPIONs were used in this work.

Control cells were incubated with fresh culture medium. All extract media and controls were seeded in five separate wells. In order to avoid contamination in the cell culture, filter-sterilization (Whatman syringe filter with pore size of 220 nm) of liquids con-

taining the SPION was applied before introducing the liquid to the cell medium. The SPIONs were easy to sterile filtrate; no detectable amount of particles was lost during this procedure.

In order to reduce the HCl component source, the modified medium, in which pH regulation is done by sodium bicarbonate, was also used.

2.2.1. MTT assay

Cytotoxicity was assessed using the MTT assay, which is a non-radioactive, colorimetric assay [32]. After 24, 48, and 72 h of incubation with extract medium, 100 μl of MTT (0.5 mg/ml) was added to each well. Following incubation, the medium was removed and the formazan crystals were solubilized by incubating for 20 min in 150 μl of isopropanol. The absorbance of each well, which identifies the quantity of viable cells, was read at 545 nm on a microplate reader (Stat Fax-2100, AWARENESS, Palm City, USA).

2.2.2. Outlier detection

All MTT experiments were performed in triplicate or more, with the results expressed as mean ± standard deviation. The standard deviation values are indicated as error bars in the MTT plots to follow. The results were statistically processed for outlier detection using a "T procedure" see, e.g., [33] using MINITAB (Minitab Inc., State College, PA). In this method, a *T*-ration is calculated as follows:

$$T = \frac{X - \bar{X}}{S}$$

where X is the suspected outlier point (normally the smallest or the largest value in a set of measurements), $\bar{X}$ is the sample mean, and S is the (estimated) standard deviation. If the calculated value of T is equal to or exceeds a critical value, the outlier point is removed with a significance level of 0.05. In the latter case, assuming that the data were sampled from a normal distribution, there is at least a 95% chance that the suspected point is in fact far from other points. For the comparison of the mean values of two or more independent populations, a one-way analysis of variance (ANOVA) was used in MINITAB. The procedure was repeated for both the conventional and the new, modified MTT assays

2.2.3. UV/vis spectroscopy

In order to investigate the compositional changes of the cell medium, UV/vis spectroscopy of the samples was measured with a Lambda 950 spectrophotometer (PerkinElmer, USA) from 260 to 850 nm wavelengths. Since the color of DMEM medium was significantly affected by minute pH changes, UV/vis seems to be a suitable method during interactions with SPIONs at wavelength of 560 nm.

2.2.4. Crystal violet staining

The cell culture medium was removed carefully from the wells and the cells washed gently with PBS at room temperature. The crystal violet dye, 100 μl of a solution (including 0.5 mg of 0.5% crystal violet (toxic), 20 μl of 20% methanol, dH_2O 80 μl) was added, incubated for 10 minutes at room temperature, and washed off with PBS before imaging.

3. Results and discussion

3.1. Characteristics of the prepared SPIONs

Fig. 1 shows TEM images of uncoated and coated SPION. For the coated nanoparticles, magnetic beads with diameters between 20 and 30 nm are formed, while single aggregated nanoparticles are observed for the uncoated iron oxide nanoparticles. The composition of magnetite is confirmed via selected area electron diffraction

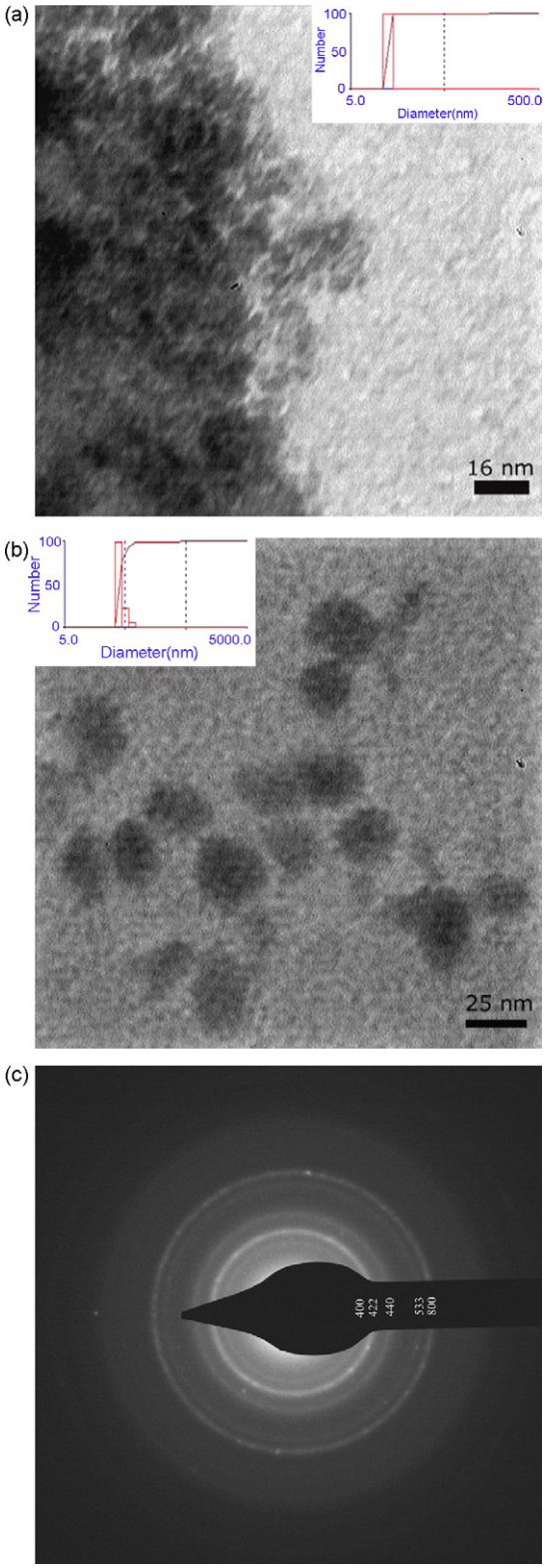

Fig. 1. TEM images of (a) uncoated (average size of 12.5 nm confirmed by DLS) and (b) coated nanoparticles (average size of 28 nm confirmed by DLS). (c) Selected area electron diffraction showing the magnetite crystal lattice.

(SAED) (Fig. 1(c)). Fig. 2 shows XRD patterns of the uncoated and coated nanoparticles. The full width at half maximum (FWHM) of the (3 1 1) reflection was used to determine the average crystallite size of the nanoparticles using the Scherrer method. The average size of SPIONs is 3.8 nm for both uncoated and coated nanoparti-

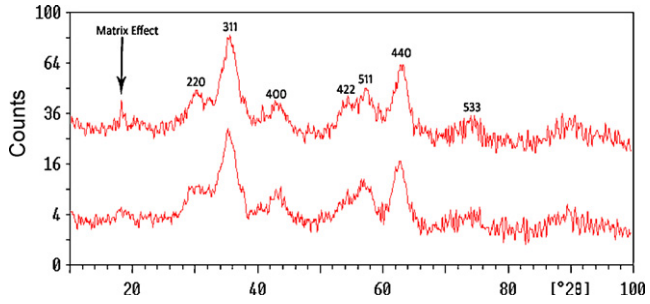

Fig. 2. XRD patterns of uncoated (lower) and coated (upper) magnetite nanoparticles.

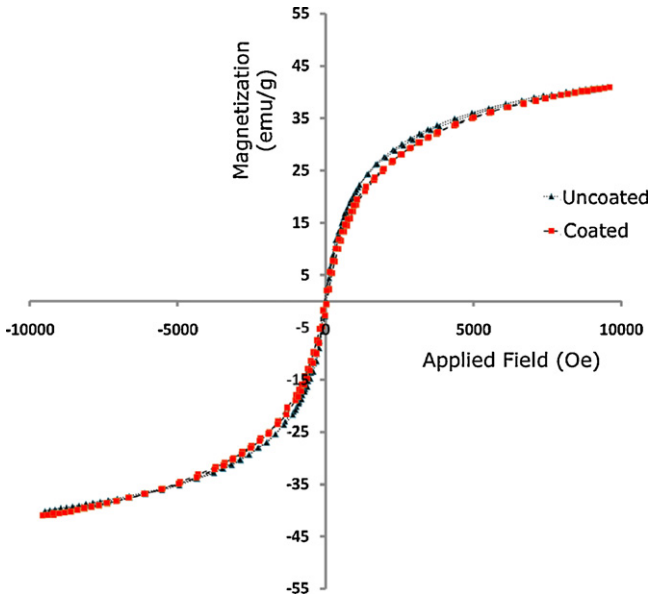

Fig. 3. Magnetization curves for uncoated and coated magnetite nanoparticles.

cles. The formation of magnetic beads in coated nanoparticles is confirmed not only by a comparison between the size of particles in TEM images and XRD results, but also by the decrease in saturation magnetization amounts. In addition, a trace of magnetic beads is detected at 18° [22]. The samples analyzed by VSM show superparamagnetic behavior. Fig. 3 illustrates the hysteresis loops of the synthesized nanoparticles, showing a negligible remanence and coercivity in the hysteresis loops. In previous work, we hypothesized that PVA is chemisorbed to the surface of SPION [22]. The chemisorption may involve hydrogen bonding [34].

3.2. Variations in cell culture medium composition

It is well-known that the surface of materials in a biological environment is covered by biomolecules (e.g., proteins) [35–45]. Consequently a cellular response to a material in a cell medium can

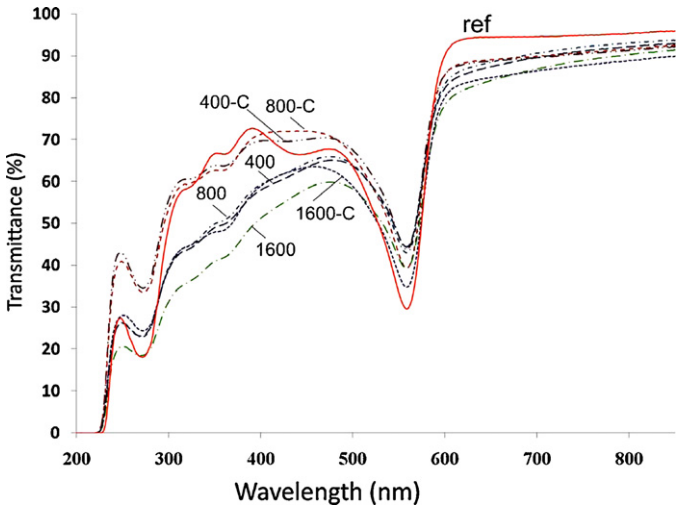

Fig. 4. UV/vis spectrum of original cell medium (i.e., ref), the extract of coated (C) and uncoated SPION against DI water as reference. The numbers refer to the millimolarity of the SPION that have been added to the cells.

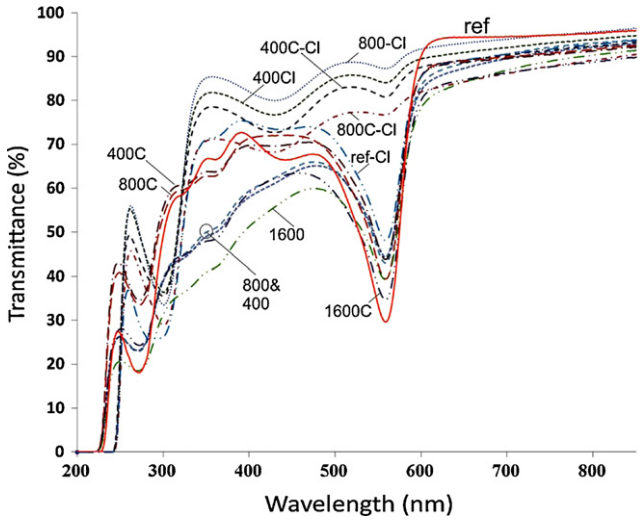

Fig. 5. UV/vis spectrum of pure cell medium (ref), the extract of coated and uncoated SPION as well as Cl ion treated medium when DI water recognized as reference.

Table 1
Zeta potential for uncoated and coated SPIONs before and after interactions with the cell medium.

SPION	Serum	Zeta potential (mV)
Uncoated	–	−21.14
Uncoated	+	+16.32
Coated	–	+3.21
Coated	+	+10.2

Table 2
Description of sample's abbreviations (e.g., B in 1600B).

Sample	Description
B	Bare nanoparticles
E	Extract of the cell medium after interaction with bare nanoparticles
C	Coated nanoparticles
CE	Extract of the cell medium after interaction with coated nanoparticles
M	Surface saturated bare nanoparticles (after interaction with DMEM)
ME	Extract of the cell medium after interaction with surface saturated bare nanoparticles
CM	Surface saturated coated nanoparticles (after interaction with DMEM)
CME	Extract of the cell medium after interaction with surface saturated coated nanoparticles

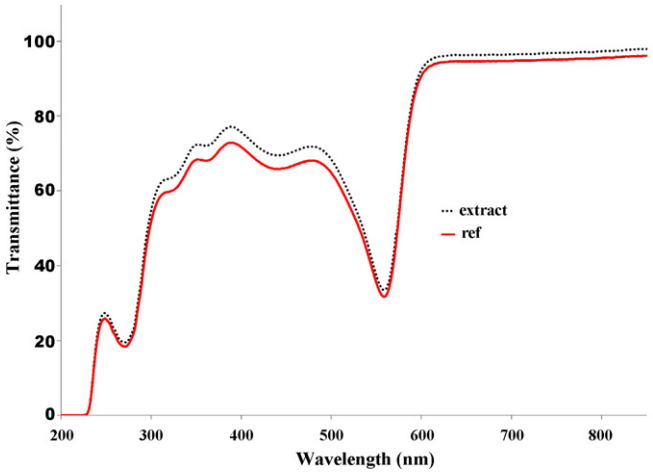

Fig. 6. UV/vis spectrum of pure cell medium (ref) and the extract from the medium interated with surface saturated SPION.

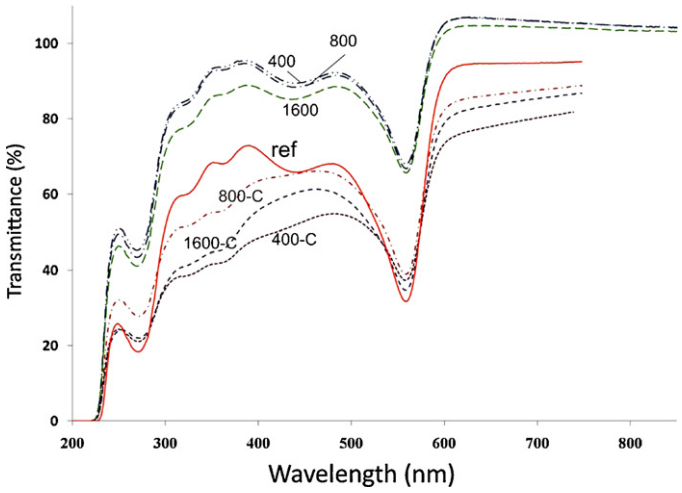

Fig. 8. UV/vis spectrum of 'modified' cell medium (ref), the extract of coated (C) and uncoated SPION in modified medium when DI water defined as reference in UV/vis spectrum.

reflect the properties of adsorbed biomolecule layers and be used for comparisons to the material itself [35,37,40,45]. Also, it has been recognized that the biomolecule layers would be able to define the biological identity of the nanoparticles [37]. Iron oxides are often negatively charged in water due to adsorption of OH^- groups on the surface of SPIONs. Surface charges give rise to an electric field and this will attract counter ions. The layer of surface charges and counter ions make up the electric double layer [46]. The attraction of the electric field is decreased for the coated nanoparticles due to a reduction in amount of the surface charge [46]. As a result, both uncoated and coated nanoparticles are susceptible, though to different extents, to protein adsorption.

During the MTT assay, the SPIONs are added to DMEM which contains many sources of proteins, vitamins, amino acids, etc. in fetal bovine serum. For example, the amount of chloride ions, which play an important role in the homeostasis of biological systems, is a good candidate for probing after exposure of SPIONs in DMEM. It is worth adding that the maximum and minimum amount of Cl^- that the cells may tolerate is reported to be 130 and 70 mM (normal range: 103–112 mM), respectively [47] and these amounts existed in the composition of DMEM medium under consideration. We hypothesized that chloride ions may be able to attach to Fe in competition with the hydroxyl groups. As a result, not only the amount of Cl^- ions is decreased in the diffuse double layer of SPION in the DMEM medium, but also the composition of the DMEM medium can be changed due to the attraction of proteins, amino acids, and vitamins in the diffuse double layer. Cedervall et al. [36] showed that the particle characteristics (i.e., size, charge and hydrophobicity) can significantly effect the proteins affinity to the surface

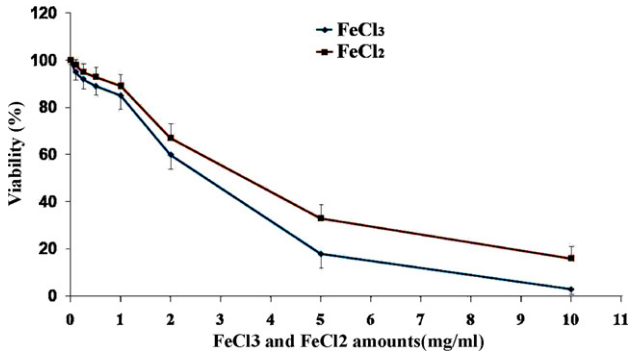

Fig. 7. Viability of the L929 cells measured by the MTT assay after 3 days of incubation with different concentrations of $FeCl_3$ and $FeCl_2$.

of nanoparticles. As a result, there could be significant differences between coated and uncoated nanoparticles due to their different surface characteristics.

In order to investigate the cell medium variation due to the exposure to nanoparticles, the viabilities of cells in samples with both uncoated and polymer coated SPIONs were studied. It is found that the viabilities of coated SPIONs are higher than those of uncoated SPIONs (see Section 3.4). This may be due to a lower biomolecule affinity (along with their denaturation) and the ability to change the surrounding milieu. In addition, the lower and positive electric surface charges on the coated SPIONs denote fewer available sites for biomolecules to attach, in comparison to the uncoated SPIONs. To support this indication, Table 1 shows the zeta potential variation measured before and after interactions of both types of SPIONs with the cell medium. From the significant zeta potential variation, it is concluded that a biomolecular layer is formed on the surface of both bare and coated nanoparticles. Next, the UV/vis measurements were conducted. A significant amount of coated and uncoated SPIONs was introduced to the cell medium (400, 800 and 1600 mM). Table 2 shows the description of the applied samples. Fig. 4 illustrates the UV/vis results of different extracts of cell mediums containing coated and uncoated SPION after 24 h. Clear changes in the medium spectra are detected between 250 and 500 nm and at 560 nm. Differences in the UV/vis spectra of the SPIONs at $\lambda = 560$ nm can be related to pH variations in the medium. In turn, the affinity of proteins to the surface of nanoparticles is highly dependent on these variations [48] and as a result, the new composition may cause cell death during *in vitro* examinations.

In order to investigate the Cl^- ion adsorption on the surface of SPIONs from the changes in the pH, the same amount of $AgNO_3$ solution (0.1 M) was introduced to equal quantities of pure and extracted cell media. Differences between the spectra of pure and extracted cell media were revealed in the UV/vis spectra (Fig. 5), suggesting that SPIONs can affect the chloride amount in DMEM. It is noteworthy that the changes from coated SPIONs are lower than from uncoated SPIONs for the same molarity, which may indicate a lower tendency of coated SPIONs to adsorb Cl^- ion.

In order to investigate the saturation of available sites for proteins on the surface of SPIONs, 1600 mM of uncoated SPIONs were introduced into fresh cell medium. After 24 h of interaction, the nanoparticles were collected by centrifugation at 2000 × *g* and then re-dispersed in fresh cell medium. After another 24 h, the modified particles were removed by centrifugation and the extract trans-

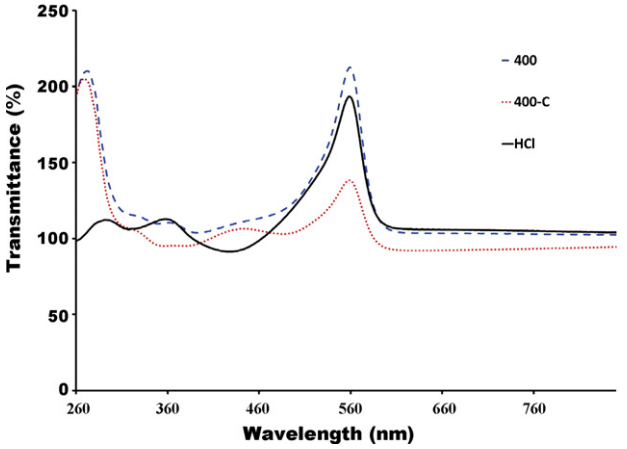

Fig. 9. UV/vis spectrum of the medium with 400 μl HCl (37%), the extract of coated (C) and uncoated SPION (iron concentration of 400 mM) in modified medium when cell medium defined as reference in UV/vis spectrum.

ferred for UV/vis spectroscopy observation. No significant changes were detected between the fresh media and the extract. Fig. 6 demonstrates the UV/vis of the pure cell medium in contrast with that of the extracted cell medium. From these data, it is found that the affinity of biomolecules to the surface of saturated nanomaterials is significantly decreased in comparison to unsaturated one. As a result, the cellular response to the surface saturated materials in biological media can reflect the toxicity of the material itself. The surface saturated materials appeared to be less toxic.

The maximum, average and minimum amounts of Cl^- in mg/ml were calculated (2.21, 1.7 and 1.19 mg/ml, respectively). As a result, the maximum changes for an ideal medium would be 0.5 mg/ml (1.7 ± 0.5 mg/ml). Fig. 7 shows the effect of the Cl^- concentrations on the viability of L929 cells. The control incubation of the cells with $FeCl_3$ and $FeCl_2$ solutions shows a small effect on the cells growth (Fig. 7). At concentrations below 0.005 and 0.01 mg/ml for $FeCl_3$ and $FeCl_2$, respectively, no toxicity is observed. Häfeli and Pauer [23] have reported that this effect is related to the iron concentration. In this experiment, due to the varying amount of Cl^- while the amount of iron in $FeCl_3$ and $FeCl_2$ was held constant, it appears that Cl^- ions may play a role in the toxicity.

In order to reduce the effect of HCl on the cell medium, a modified DMEM was used. In the modified medium, sodium bicarbonate was used instead of HCl to adjust the pH value. The results of using this modified medium are illustrated in Fig. 8. Changes in the DMEM composition in the range of 260–500 nm are decreased slightly and the same behavior of the cell medium is observed. Hence, we deduce that the biomolecule–nanoparticle interactions have a dominant effect on the variation of cell medium. The modified medium is more reliable for *in vitro* examinations since sodium bicarbonate is applied in order to adjust the pH value.

Finally, in order to investigate the effect of pH reduction without biomolecular interactions in the UV/vis spectrum, 400 μl of 1 M HCl were introduced to 6 ml DMEM. The results are illustrated in Fig. 9. Differences between samples concentrated at a wavelength of 560 nm are seen, which are attributed to an increase of H^+ in the solution. No changes are observed at wavelengths between 260 and 300 nm (the range of protein interactions). Hence, it appears that

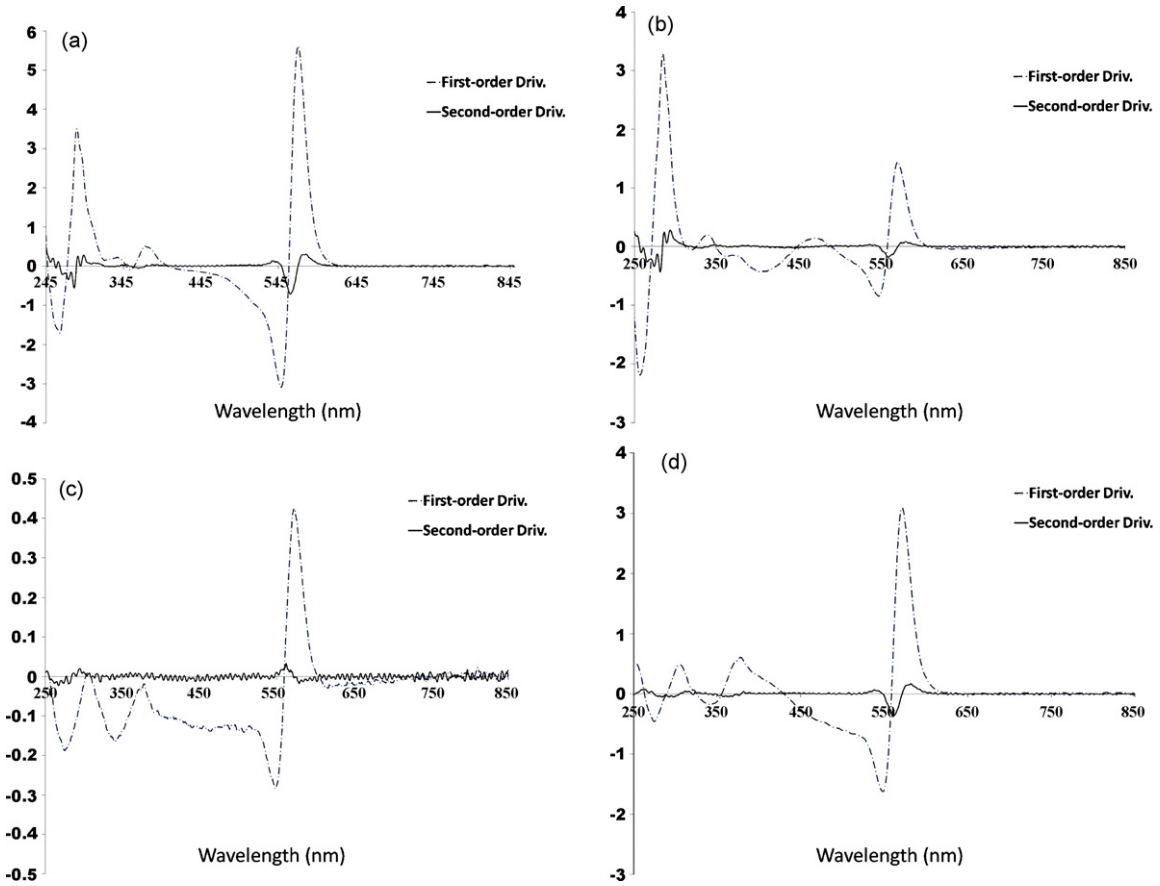

Fig. 10. First (dash-line) and second (solid line) order derivatives of (a) 1600B, (b) 1600C, (c) 1600CM (modified sample) and (d) medium with HCl (ref conventional DMEM).

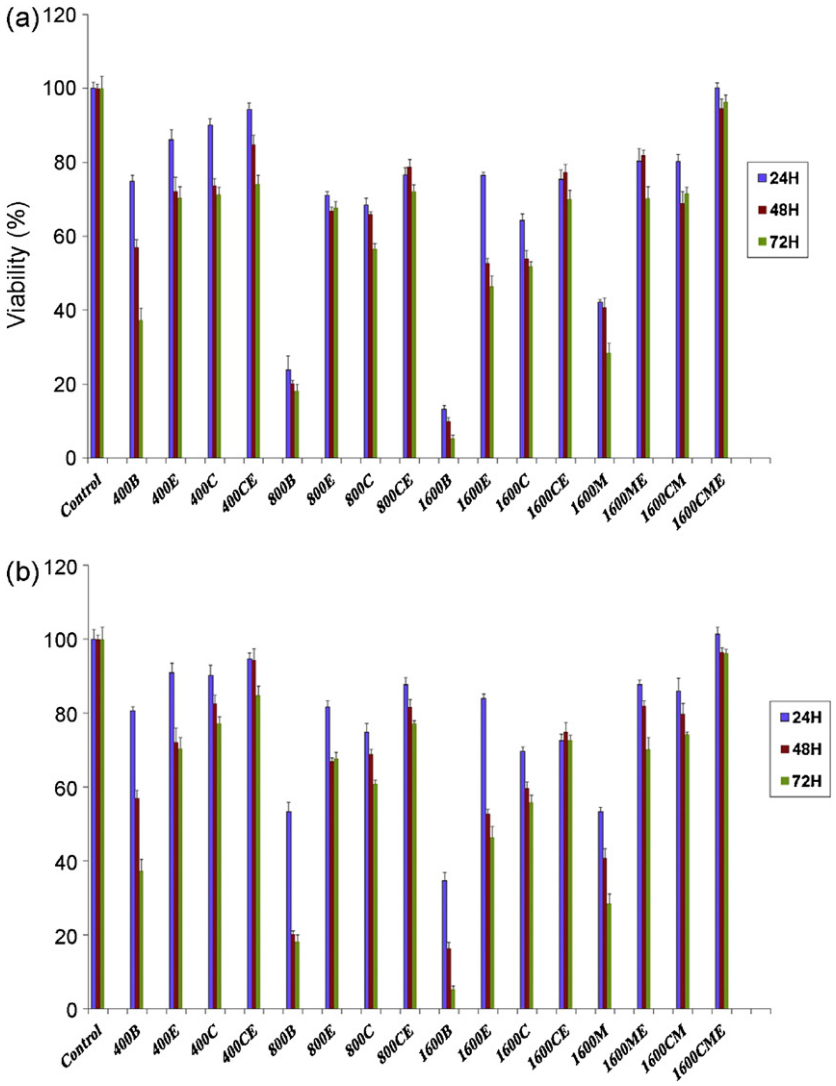

Fig. 11. MTT assay values for L929 using (a) conventional and (b) modified DMEM (B, E, C, M refers to uncoated (i.e., bare), extract, coated and modified, respectively).

many moieties in DMEM, such as proteins, have been adsorbed on the surface of SPIONs.

3.3. Derivative spectroscopy

The broad bands and shoulders in the UV/vis results arise from the overlap of adjacent peaks, which cannot be fully resolved even with the highest performance spectrophotometers. In many instances the UV/vis spectroscopic technique is not specific enough to characterize adequately individual molecular compounds in a solution, particularly in the presence of other adsorbing molecular species and scattering particles [49]. The derivatization of spectra can lead to more accurate determination of the wavelengths of broad peak maxima and peaks appearing only as shoulders, as well as the isolation of small peaks from interfering large background absorption. Here first and second order derivatives are used to detect the multi-component changes in DMEM medium due to the presence of SPIONs. The results are shown in Fig. 10. For uncoated nanoparticles, the pH change is larger than the coated nanoparticles (at 560 nm) due to the higher surface activity to adsorb ions and other compounds in DMEM. Multi-component adsorbance (biomolecules–nanoparticles interactions) is detected via the second derivative curves between the wavelengths of 250–300 nm in both uncoated and coated nanoparticles (Fig. 10(a) and (b)). Fig. 10(c) shows the derivative curves for the modified samples, showing negligible absorbance at aforementioned wavelengths. In order to see the effect of Cl^- in DMEM, the effect of HCl on DMEM's changes is shown in Fig. 10(d). The major effect of HCl is focused at the wavelength of 560 nm owing to a decrease in pH of the medium.

3.4. MTT results

MTT reduction was used to metabolically quantify viable cells after exposure to SPIONs. Cell detachment upon the exposure

Table 3
Comparison of viability for the 1600B sample before and after outlier removal for both conventional and modified MTT methods.

MTT method	Viability (%): before removing outliers	Standard deviation	Viability (%): after removing outliers	Standard deviation
Conventional	15.3	5.1	17.8	3.1
Modified d	30.4	3.6	34.6	2.3

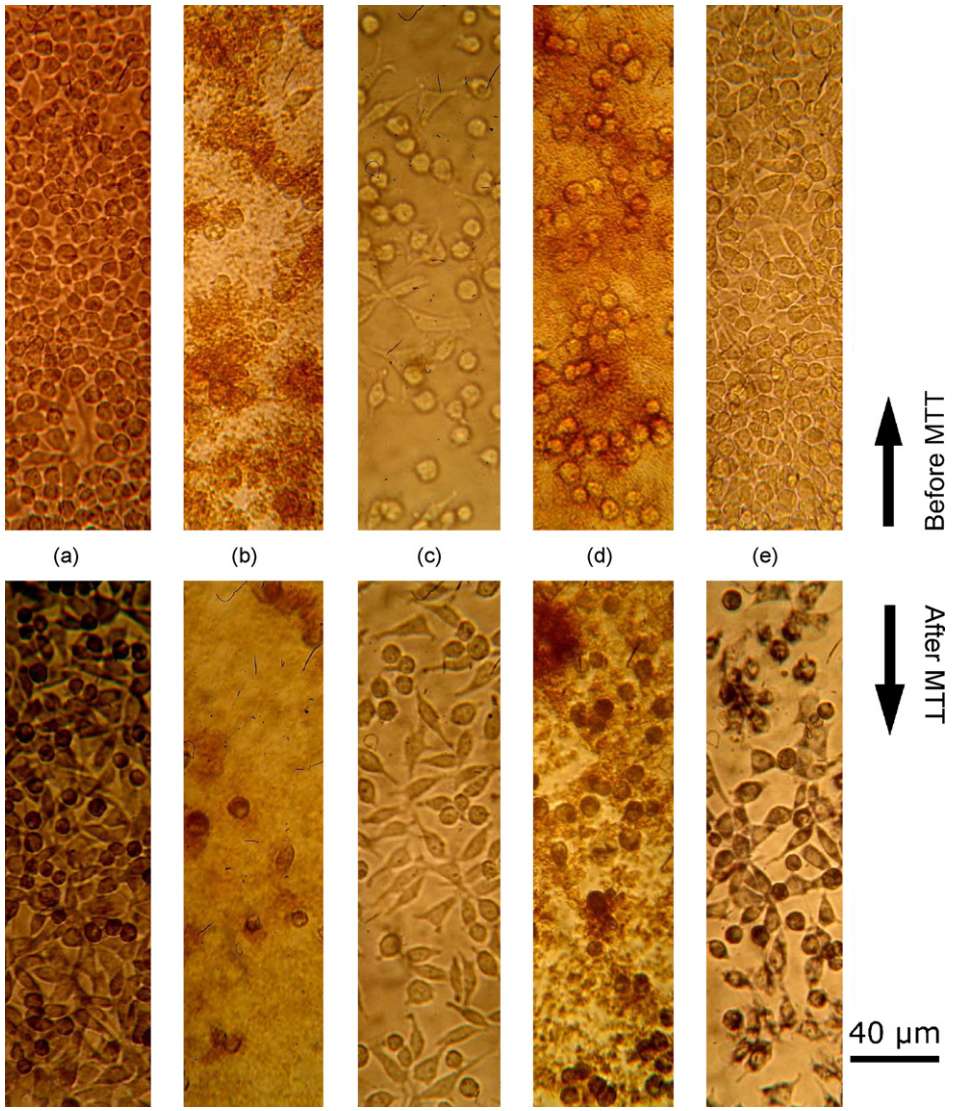

Fig. 12. Optical microscopy (400×) of L929 cells before and after MTT treatment for (a) control, (b) cells containing 1600 mM uncoated SPION, (c) extract of case (b), (d) cells containing 1600 mM modified uncoated SPION and (e) extract of case (d).

necessitated the development of customized protocols for the MTT assay; detachment is increased with both increasing SPIONs concentration and contact time, especially for uncoated nanoparticles. The coated and uncoated iron oxide nanoparticles have very different surface properties and thus, different surface reactivities. For example, magnetite (Fe_3O_4) can cause smaller toxicity effects (examined with comet assay) and larger oxidative DNA lesions in cultured A549 cells (the human lung epithelial cell line) in comparison to maghemite (Fe_2O_3) [27]. Larger DNA damage with magnetite may relate to the oxidation effect of uncoated particles; thus coated magnetite show lower DNA damage due to the fewer potential oxidative sites. The MTT assay was applied for all the examined samples and results confirm the large effect of SPIONs on the DMEM (see Fig. 11(a)). The extracts of the cell medium with SPIONs show toxicity due to increasing amounts of H^+ as well as compositional changes in DMEM. Further, the modified SPIONs show significant enhancements in cell viability on both uncoated and coated particles with different SPION molarity. This effect may be due to the saturation of sites on the surface of SPIONs, leaving limited sites for biomolecules adsorption to the surface of nanoparticles. The quantitative values of the errors obtained via the conventional and modified methods (i.e., using surface saturated nanoparticles) after outlier removal are 27.3 ± 3.8 and 16.3 ± 2.5 for uncoated and coated nanoparticles, respectively. Table 3 shows the results for 1600 mM of uncoated SPIONs before and after outlier removal. Fig. 11(b) illustrates the MTT results for the modified medium (i.e., using sodium bicarbonate instead of HCl), confirming a slightly better viability due to the decreased HCl amount in the medium. To probe the shape or morphology changes due to the exposure of cells to SPIONs in the monolayer culture, optical microscopy was used. Results for L929 cells without staining are illustrated in Fig. 12.

In order to see the morphology of damaged cells due to the presence of the uncoated SPIONs, the cells were exposed to crystal violet. The morphology of the cells is illustrated in Fig. 13. It can be observed that gas vesicles are present inside the cells due to the presence of SPIONs. Gas vesicles are the components of gas vacuoles, which were discovered in cells of bloom-forming cyanobacteria in water by German microbiologists nearly a century ago [50,51]. Klebahn [52] showed that gas vacuoles provide cells with buoyancy [53,54]. The vesicles are used by archaea, bacteria and planktonic microorganisms, possibly to (a) control vertical migration by regulating the gas content and thereby buoy-

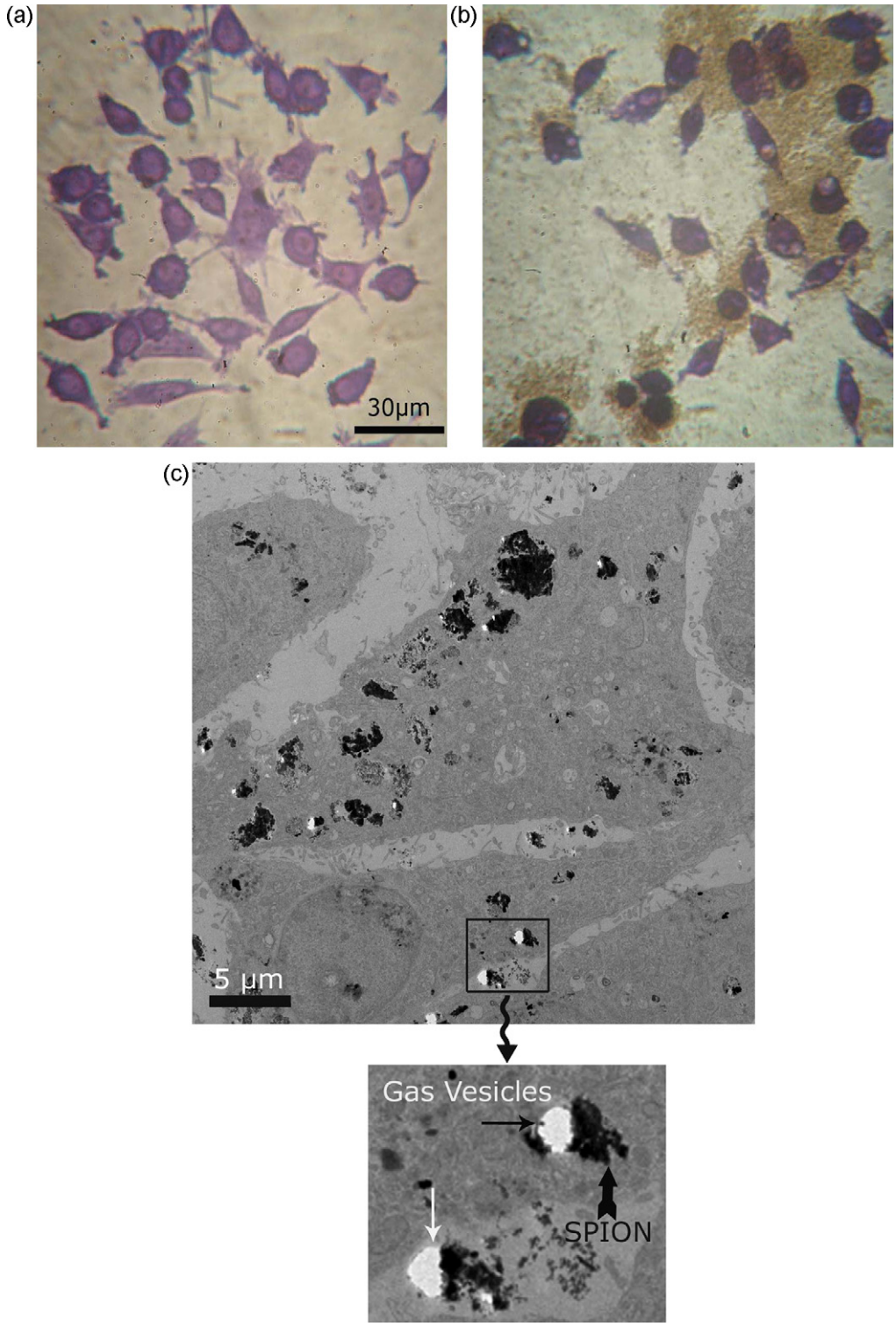

Fig. 13. Optical microscopy (800×) of dyed L929 cells for (a) control, (b) cells containing 800 mM uncoated SPION after 72 h interaction with cells. (c) TEM images of SPION-treated cells showing gas vesicles.

ancy, and (b) position the cell for maximum solar light harvesting [49].

In our study, TEM images from the vesicles revealed the existence of SPIONs inside. It appears that bubble formation is responsible for toxicity of SPIONs due to the local changes in protein function as well as ionic equilibrium. No gas vesicles were observed with the addition of surface saturated (modified) SPIONs to cells even in the concentration of 1600 mM. Mahmoudi et al. [55] previously found a severe detachment of SPION-treated L929 cells. From our finding in the present work, this phenomenon can now be explained by the formation of gas vesicles. It is surprising to see that gas vesicles are detected in SPION-treated cells due to the protein–nanoparticle interactions and further efforts will be directed towards this phenomenon to better understand and eventually prevent the toxicity effects of the nanoparticles.

4. Conclusion

The core hypothesis of this study was to make a direct correlation between *in vitro* and *in vivo* studies by understanding the effect of nanoparticles on the cell medium, in particular the interaction of nanoparticles with biomolecules. The effects of both PVA coated and uncoated superparamagnetic iron oxide nanoparticles on the cell medium were examined. It is shown that the conventional *in vitro* examination method may contain large errors as compared to the modified method. This may be partially attributed to the fact that SPIONs can cause significant changes in the cell medium, such as denaturation of proteins, which in turn can cause toxicity. The modified method is:

- Introduction of the nanoparticles to the cell medium.
- Leaving the solution in contact for a period of 24 h.
- Replacing the medium with a fresh one.
- Application of the surface saturated SPIONs to the assays.

Using this approach, the toxicity of uncoated SPIONs is found to decrease significantly. It is also observed that the existence of chloride may increase the error magnitudes in the conventional *in vitro* method. Coated nanoparticles induce lower toxicity not only due to the presence of the biocompatible coating, but also due to the lower adsorption sites for proteins, ions and other components in medium. Regarding crystal violet dye, it is hypothesized that the toxicity of SPIONs is partly related to inducing gas vesicle formation.

References

[1] C. Alexiou, W. Arnold, R.J. Klein, F.G. Parak, P. Hulin, C. Bergemann, W. Erhardt, S. Wagenpfeil, A.S. Lübbe, Cancer Res. 60 (2000) 6641–6648.
[2] C. Alexiou, R. Jurgons, R. Schmid, A. Hilpert, C. Bergemann, F. Parak, H. Iro, J. Magn. Magn. Mater. 293 (2005) 389–393.
[3] Y. Weizmann, F. Patolsky, E. Katz, I. Willner, J. Am. Chem. Soc. 125 (2003) 3452–3454.
[4] H.T. Song, J.S. Choi, Y.M. Huh, S.J. Kim, Y.W. Jun, J.S. Suh, J.W. Cheon, J. Am. Chem. Soc. 127 (2005) 9992–9993.
[5] M. Mahmoudi, A. Simchi, M. Imani, U.O. Häfeli, J. Phys. Chem. C 113 (19) (2009) 8124–8131.
[6] Y. Chen, L.S. Yang, C. Feng, L.P. Wen, Biochem. Biophys. Res. Commun. 337 (2005) 52–60.
[7] L.M. Zhang, K.Q. Zhang, R. Prandl, F. Schoffl, Biochem. Biophys. Res. Commun. 322 (2004) 705–711.
[8] Y. Chen, J. Aveyard, R. Wilson, Chem. Commun. 24 (2004) 2804–2805.
[9] N. Jessel, F. Atalar, P. Lavalle, J. Mutterer, G. Decher, P. Schaaf, J.C. Voegel, J. Ogier, Adv. Mater. 15 (2003) 692–695.
[10] H.J. Qiu, J. Rieger, B. Gilbert, R. Jerome, C. Jerome, Chem. Mater. 16 (2004) 850–856.
[11] H.A. Jeng, J. Swanson, J. Environ. Sci. Health A: Toxicol. Hazard. Subst. Environ. Eng. 41 (2006) 2699–2711.
[12] M. Mahmoudi, A. Simchi, M. Imani, J. Phys. Chem. C 113 (22) (2009) 9573–9580.
[13] S.M. Hussain, K.L. Hess, J.M. Gearhart, K.T. Geiss, J. Schlager, J. Toxicol. In Vitro 19 (2005) 975–983.
[14] M. Mahmoudi, A. Simchi, A.S. Milani, P. Stroeve, Colloid Interface Scie. 336 (2) (2009) 510–518.
[15] J.M. Veranth, E.G. Kaser, M.M. Veranth, M. Koch, G.S. Yost, Part. Fibre Toxicol. 4 (2007) 2.
[16] H. Hosseinkhani, M. Hosseinkhani, Curr. Drug Saf. 4 (2009) 79–83.
[17] H. Hosseinkhani, M. Hosseinkhani, N.P. Gabrielson, D.W. Pack, A. Khademhosseini, H. Kobayashi, J. Biomed. Mater. Res. A 85 (2008) 47–60.
[18] H. Hosseinkhani, Int. J. Nanotechnol. 3 (2006) 416–461.
[19] G.A. Hughes, Clin. Cancer Res. 14 (2008) 1310–1316.
[20] K. Cho, X. Wang, S. Nie, Z. Chen, D.M. Shin, Nanomedicine 1 (2005) 22–30.
[21] U.O. Häfeli, G.J. Pauer, J. Magn. Magn. Mater. 194 (1999) 76–82.
[22] J. Sun, S. Zhou, P. Hou, Y. Yang, J. Weng, X. Li, M. Li, J. Biomed. Mater. Res. A 80 (2007) 333–341.
[23] K. Donaldson, V. Stone, A. Seaton, W. MacNee, Health Perspect. 109 (2001) 523–527.
[24] N. Li, M. Hao, R.F. Phalen, W.C. Hinds, A.E. Nel, Clin. Immunol. 109 (2003) 250–265.
[25] H.L. Karlsson, P. Cronholm, J. Gustafsson, L. Moller, Chem. Res. Toxicol. 21 (2008) 1726–1732.
[26] C.M. Sayes, K.L. Reed, D.B. Warheit, Toxicol. Sci. 97 (2007) 163–180.
[27] A. Moore, E. Marecos, A. Bogdanov Jr., R. Weissleder, Radiology 214 (2) (2000) 568–574.
[28] F.K.H. Landeghem, K. Maier-Hauff, A. Jordan, K.T. Hoffmann, U. Gneveckow, R. Scholz, B. Thiesen, W. Brück, A. Deimling, Biomaterials 30 (2009) 52–57.
[29] http://en.citizendium.org/wiki/Kidney.
[30] M. Mahmoudi, A. Simchi, M. Imani, A.S. Milani, P. Stroeve, J. Phys. Chem. B 112 (46) (2008) 14470–14481.
[31] A. Petri-Fink, M. Chastellain, L. Juillerat-Jeanneret, A. Ferrari, H. Hofmann, Biomaterials 26 (2005) 2685–2694.
[32] R. Pieters, D.R. Huismans, Br. J. Cancer 59 (1989) 217–220.
[33] S. Bolton, Pharmaceutical statistics: Practical and clinical applications, 2nd Ed., Marcel Dekker, New York, 1990.
[34] H.-L. Ma, X.-R. Qia, Int. J. Pharm. 333 (2007) 177–186.
[35] I. Lynch, K.A. Dawson, S. Linse, Science STKE 327 (2006) pe14.
[36] T. Cedervall, I. Lynch, S. Lindman, T. Berggård, E. Thulin, H. Nilsson, K.A. Dawson, S. Linse, Proc. Natl. Acad. Sci. U.S.A. 104 (2007) 2050–2055.
[37] W. Norde, J. Lyklema, Biomater. Sci. Polym. Ed. 2 (1991) 183–202.
[38] W. Norde, D. Gage, Langmuir 20 (2004) 4162–4167.
[39] L.T. Allen, M. Tosetto, I. Miller, D. O'Connor, S.C. Penney, I. Lynch, A.K. Keenan, S.R. Pennington, K.A. Dawson, W.M. Gallagher, Biomaterials 27 (2006) 3096–3108.
[40] J.J. Gray, Curr. Opin. Struct. Biol. 14 (2004) 110–115.
[41] C.J. Wilson, R.E. Clegg, D.I. Leavesley, M.J. Pearcy, Tissue Eng. 11 (2005) 1–18.
[42] M.F. Engel, A.J.W.G. Visser, C.P. van Mierlo, Proc. Natl. Acad. Sci. U.S.A. 101 (2004) 11316–11321.
[43] M. Shen, J. Biomed. Mater. Res. A 70 (2004) 533–541.
[44] C.S. Chen, E. Ostuni, G.M. Whitesides, D.E. Ingber, Methods Mol. Biol. 139 (2000) 209–219.
[45] I. Lynch, K.A. Dawson, Nanotoday 3 (1–2) (2008) 40–47.
[46] H.-J. Butt, K. Graf, M. Kappl, Physics and Chemistry of Interfaces, Wiley-VCH, Weinheim, 2003.
[47] A.C. Guyton, Text Book of Medical Physiology, 11th ed., W.B. Saunders Co., Philadelphia, 2006.
[48] A.L. Lehninger, Biochemistry, Worth Publishers, Inc., New York, NY, 1970.
[49] K.G. Jones, G.D. Sweeney, Biochem. Med. 15 (1976) 223.
[50] M. Blank, F.J.W. Roughton, Trans. Faraday Soc. 56 (1960) 1832–1841.
[51] A.E. Walsby, Microbiol. Rev. 58 (1994) 94–144.
[52] H. Klebahn, Flora, Jena 80 (1895) 24–257.
[53] H. Klebahn, Jahrb. Wiss. Bot. 61 (1922) 535–589.
[54] H. Klebahn, Int. Ver. Limnol. 4 (1929) 408–414.
[55] M. Mahmoudi, M.A. Shokrgozar, A. Simchi, M. Imani, A.S. Milani, P. Stroeve, H. Vali, U.O. Häfeli, S. Bonakdar, J. Phys. Chem. C 113 (6) (2009) 2322–2331.